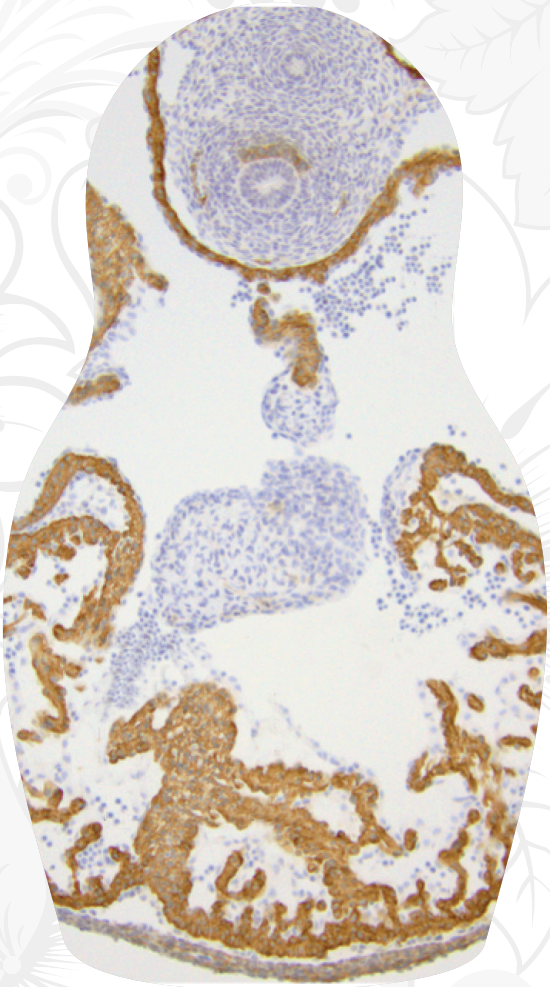

Chapter 5

Lack of Primary Cilia Primes Shear-Induced Endothelial-to-Mesenchymal Transition

Anastasia D. Egorova[1], Padmini P.S.J. Khedoe[1,2], Marie-José T.H. Goumans[3], Bradley K. Yoder[4], Surya M. Nauli[5], Peter ten Dijke[3], Robert E. Poelmann[1], Beerend P. Hierck[1]

[1]Department of Anatomy and Embryology, Leiden University Medical Center, Leiden, The Netherlands. [2]Present address: Department of Pulmonology, Leiden University Medical Center, Leiden, The Netherlands. [3]Molecular Cell Biology and Center for Biomedical Genetics, Leiden University Medical Center, Leiden, The Netherlands. [4]Department of Cell Biology, University of Alabama at Birmingham, Alabama, USA. [5]Pharmacology and Medicine, College of Pharmacy and Medicine, University of Toledo, Ohio, USA.

Circulation Research, 108(9): 1093-1101 (2011)

Abstract

Primary cilia are cellular protrusions that serve as mechanosensors for fluid flow. In endothelial cells (ECs), they function by transducing local blood flow information into functional responses, such as nitric oxide production and initiation of gene expression. Cilia are present on ECs in areas of low or disturbed flow and absent in areas of high flow. In the embryonic heart, high-flow regime applies to the endocardial cushion area, and the absence of cilia here coincides with the process of endothelial-to-mesenchymal transition (EndoMT). In this study, we investigated the role of the primary cilium in defining the responses of ECs to fluid shear stress and in EndoMT. Nonciliated mouse embryonic ECs with a mutation in Tg737/Ift88 were used to compare the response to fluid shear stress to that of ciliated ECs. *In vitro,* nonciliated ECs undergo shear-induced EndoMT, which is accompanied by downregulation of Klf4. This Tgfβ/Alk5-dependent transformation is prevented by blocking Tgfβ signaling, overexpression of Klf4, or rescue of the primary cilium. In the hearts of $Tg737^{orpk/orpk}$ embryos, Tgfβ/Alk5 signaling was activated in areas in which ECs would normally be ciliated but now lack cilia because of the mutation. In these areas, ECs show increased Smad2 phosphorylation and expression of α-smooth muscle actin. This study demonstrates the central role of primary cilia in rendering ECs prone to shear-induced activation of Tgfβ/Alk5 signaling and EndoMT and thereby provides a functional link between primary cilia and flow-related endothelial performance.

Introduction

Cilia are specialized membrane covered rod-like organelles protruding from virtually all mammalian cells[1]. Primary cilia are typically present as solitary cellular extensions and are generally immotile, with the exception of cilia on the primitive node of the vertebrate embryo[2]. Interest in the (dys) function of primary cilia arose because of their role in olfaction, photoreception, chemosensation, and mechanosensation[3]; their association with a number of human ciliopathies[1,4]; and their function as cellular sensory antennae. Biological effects include coordination of cell proliferation and differentiation. Ciliary structure, assembly, and maintenance is dependent on microtubule-based motor transport of axoneme subunits from the body of the cell into ciliary tips using a bidirectional process termed intraflagellar transport (IFT). Mutations in many of the IFT components lead to defective ciliogenesis[5] and are associated with a range of human pathologies, such as Orofaciodigital, Bardet-Biedl, Usher, Senior-Loken, and Jeune syndromes. These syndromes can include laterality defects, vestibular impairment, and polycystic kidney disease[1,4–6].

Endothelial cells lining the heart and blood vessels are constantly exposed to hemodynamic forces, of which shear stress represents the drag force on the endothelium exerted by blood flow. The differential response of endothelial cells (ECs) to constantly varying flow patterns and velocities requires accurate mechanosensing and mechanotransduction. Primary cilia can sense shear stresses as low as 0.0007 Pa[7], and they function as flow sensors in kidney epithelium[8], bone matrix lacunae osteocytes and osteoblasts, bile duct epithelium, and vascular endothelium[9,10]. The function of primary cilia in endothelial shear sensing appears to be biphasic. Fluid flow and the associated ciliary deformation lead to a polycystin-mediated intracellular Ca^{2+} transient within seconds[9,11]. Furthermore, the cilium is considered to amplify the cytoskeletal strain, resulting in a prolonged effect on gene expression of shear-responsive genes, including *Krüppel-like factor* (*KLF*)[2,10,12] which further coordinates a major part of the phenotypic response of ECs to shear forces.

KLF2 and KLF4 are shear-sensitive transcription factors that have been described to coordinate the regulation of endothelial function and the establishment of a quiescent, antiinflammatory, and antithrombotic phenotype[13–16]. Recent studies point toward a significant degree of mechanistic and functional overlap between KLF2 and KLF4 in ECs[16]. Shear stress–induced expression of *KLF2* has been shown to be related to the presence of primary cilia[9,10], and recent work suggests that cells with abnormal ciliary function or structure are likely to fail to respond to fluid shear stress appropriately[9].

Primary cilia are present on ECs during embryonic[17,18] and adult[19] life, and their distribution has been described to be spatiotemporally linked to shear stress patterns *in vivo*. In adult vasculature, primary cilia are located at atherosclerotic predilection sites where flow is low and oscillatory[19]. Moreover, ECs in areas where shear stress is high are devoid of cilia[19]. In the embryonic heart, the presence of

ciliated ECs is also restricted to areas of low and oscillatory flow, marked by low levels of *KLF2*[17,20,21]. The endocardial cushions are exposed to high shear stress[22] and show high expression of *KLF2* in the ECs[20]. Interestingly, these ECs are nonciliated[17] and undergo transforming growth factor (Tgf) β-driven endothelial-to-mesenchymal transition (EndoMT), during which ECs transdifferentiate to gain a mesenchymal phenotype and migrate into the cardiac jelly to form the primordia of cardiac valves[23]. EndoMT is marked by activation of the Tgfβ type I receptor Alk5[24,25], induction and activation of the transcription factor Snail (Snai1), loss of EC markers like CD31, and gain of expression of mesenchymal markers including α-smooth muscle actin (αSMA) and N-cadherin[26,27].

In this study, we used transgenic embryonic ECs from the *IFT88Tg737RPW* (or *Tg737*$^{orpk/orpk}$) mouse, which lack primary cilia[9]. These were used to investigate the role of the primary cilium in the response of ECs to fluid shear stress and Tgfβ and in EndoMT. Shear stress triggered EndoMT in nonciliated ECs, but not in ciliated cells, a process that depended on Tgfβ signaling and Klf4 regulation. Furthermore, we analyzed the hearts of wild-type (WT) and *Tg737*$^{orpk/orpk}$ embryos to address the consequences of the lack of endothelial cilia *in vivo*. ECs lining areas of low shear stress showed enhanced Tgfβ/Alk5 signaling activation and increased expression of the mesenchymal marker αSMA, suggesting that the lack of cilia primes the ECs for shearinduced activation of Tgfβ signaling and EndoMT.

Methods

Cell culture and supplements

Generation of mouse embryonic wild type ECs (WT) and mouse embryonic ECs with a mutation in the *Tg737* gene (*IFT88Tg737RPW* or *Tg737*$^{orpk/orpk}$) from the Oak Ridge Polycystic Kidney mouse was previously described[9]. Cells were passaged twice a week and maintained on 1% w/v gelatin (Merck) in advanced DMEM medium (Invitrogen) supplemented with 4.5 g/L D-glucose (Invitrogen), 110 mg/L sodium pyruvate (Invitrogen), non-essential amino acids (Invitrogen), 2% (v/v) heat inactivated Fetal Calf Serum (Sigma-Aldrich Chemie), 0.5% (v/v) antibiotic/ antimyotic solution (Invitrogen), 1% (v/v) insulin, transferin, selenium supplement (Invitrogen), and 2mM L-glutamine (Invitrogen). For some of the experiments, the culture medium was supplemented with Tgfβ3 (1ng/ml), Tgfβ neutralizing antibody (α-Tgfβ, 2G7 IgG2b, 10ug/ml)[28], Alk5 kinase inhibitor SB431542 (10µmol/L in DMSO; Tocris)[29], or DMSO (Sigma).

Shear stress exposure

For the shear stress experiments, WT and *Tg737*$^{orpk/orpk}$ ECs were seeded on fixed 1% (w/v) gelatin coated coverslips and grown to confluence. ECs were subjected to 0.5 and 2.5 Pa shear stress for 2 or 24 hours at 37°C and 5% CO_2 in a re-circulation parallel plate flow system as previously reported[10]. Responses of shear-exposed cells were compared to those of static cultures. To block Alk5 kinase activity during exposure to shear stress, cells were pre-incubated with SB431542 for 1 hour and then exposed to shear stress in medium supplemented with the compound at the same concentration. 0.1% (v/v) DMSO (Sigma) served as a sham for the SB431542 experiments. To neutralize functional Tgfβ either present in the medium or produced by the cells during exposure to shear stress, cells were pre-incubated with a pan-Tgfβ neutralizing antibody for 1 hour prior to shear exposure in the presence of antibody in equal concentration. Static controls were treated identically with the omission of flow. Directly following incubation or exposure to flow, cells were fixed for immunofluorescence analysis (n=3) or lysed for RNA (n=4) or protein (n=3) isolation. Hoffman modulation contrast images were taken using Nikon Eclipse Ti inverted microscope system (20x and 40x objectives).

Constructs and transfection

The Ift88*/Tg737 expression construct encodes the Ift88 protein (90 kDa) and a 28kDa tag (mCherry, denoted by an asterisk (*)). *Tg737*$^{orpk/orpk}$ ECs were transfected with Lipofectamine (Invitrogen) according to the manufacturer's protocol. Stable cell lines were generated by drug selection using 500 µg/ml G418 (Invitrogen) to obtain *Tg737*$^{orpk/orpk}$*-Ift88**. Expression from the Ift88* construct was evaluated using Q-PCR and Western Blot analysis and compared to *Tg737*$^{orpk/orpk}$ cells which were stably transfected with pEGFP-N1 (Clontech R&D), which served as control.

Full length mouse Klf4 cDNA was amplified by PCR using F: 5'-CCCACATTAATGAGGCAGC-3' and R: 5'-GGTCACATCCACTACGTGG-3' primers and cloned under the regulatory control of the human cytomegalovirus (CMV) immediate early promoter/enhancer into pcDNA3.3 (Invitrogen). Cells were transfected 24 hours prior to the start of experiments using Lipofectamine to obtain *Tg737$^{orpk/orpk}$-Klf4*. All experiments were performed in quadruplicate (n=4). pcDNA3.3-LacZ (Invitrogen) served as control.

Immunocytochemistry

Cells were fixed with 4% paraformaldehyde in 0.1mol/L phosphate buffer (pH7.4) for 10 minutes at room temperature. Permeabilized cells were incubated with antibody against acetylated α-tubulin (6-11B-1, 1:2000, Sigma) and αSMA (1A4, 1:1000, Sigma) for 3 hours at 37ºC, followed by incubation with FITC-labeled rabbit-anti-mouse antiserum (1:100, DAKO). For the CD31 staining, cells were incubated overnight with PECAM-1 antibody (M-20, 1:100, Santa Cruz), followed by incubation with biotin-labeled swine-anti-rabbit antiserum (1:100, DAKO) and FITC conjugated avidin (1:100, Vector labs). DAPI (1:1000, Invitrogen) was used for nuclear counterstaining and cells were mounted in ProLong Gold (Molecular Probes). Confocal scanning was performed using a Leica SP5 confocal scanning laser microscope (63x and 100x oil immersion objectives). ImageJ and Photoshop 10.0 were used for processing the data.

Q-PCR

Total RNA was isolated (RNeasy, Qiagen) and was treated with DNAse-I (Qiagen) according to the manufacturer's protocol. IScript cDNA synthesis kit (Bio-Rad) was used to reverse transcribe 500ng of RNA into cDNA. Real-time Q-PCR was performed using iQ SYBR Green Supermix (Bio-rad) in a Mx3000 real-time thermocycler (Stratagene) as described[30]. The reaction mixture consisted of the following: 1x PCR Master Mix, 1µl cDNA template, and 10 pmol of each specific primer. Gene specific primers are listed in Table 5.1. The PCR program consisted of a hot start activation step, followed by 50 cycles of 30 seconds at 95°C, 60 seconds annealing at 58°C, and 30 seconds extension at 72°C. Dissociation analysis was performed in all reactions to exclude the presence of primer-dimers and confirm the amplification of unique targets. No-template controls were used as negative controls. Relative expression levels were normalized to the housekeeping gene *GAPDH* to compensate for the differences in RNA input.

Western Blotting

Western blot analysis was performed as described[25]. Protein samples were separated on a 8% SDS polyacrylamide gel, transferred onto a nitrocellulose membrane (Hybond P; Amersham Pharmacia Biotech), and incubated overnight at 4ºC with antibody against CD31 (M-20, 1:500, Santa Cruz), Klf4 (ab34814, 1:700, Abcam), Ift88 (Polaris B1700, 1:5000)[31], phospho-Smad2 (138D4, 1:1000, Cell Signaling) and GAPDH (6C5, 1:5000, Millipore). The blots were then incubated with peroxidase-conjugated anti-rabbit (CD31, Klf4, Ift88, phospho-Smad2) and anti-mouse (GAPDH) secondary

antibody (1:1000; GE Healthcare), and developed using the ECL Plus Western blotting detection system (Thermo Scientific). Signals were quantified using densitometry and normalized to GAPDH. Western Blots shown in the Figures are representative of 3 independent experiments.

Mice

The Oak Ridge Polycystic Kidney (*Tg737*$^{orpk/orpk}$) animals were generated by a transgene insertion mutagenesis as described previously[32] and lines were maintained as heterozygous crosses on an inbred FVB/N genetic background. Animals were treated and maintained in accordance with the Institutional Animal Care and Use Committee regulations at the University of Alabama at Birmingham. Genotyping was performed as described previously[33]. E11.5 embryos were fixed overnight in 4% parafolmaldehyde in 0.1 mol/L phosphate buffer (pH7.4) and routinely processed for paraffin immunohistochemical analysis. Specimens were sectioned transversely through the heart at 10µm.

Gene of interest	Gene ID	Oligonucleotide sequence
muActa2 (αSMA)	11475	F: 5'-CATCATGCGTCTGGACTTG-3'
		R: 5'-ATCTCACGCTCGGCAGTAG-3'
muCD31	18613	F: 5'-CTCCAACAGAGCCAGCAGTA-3'
		R: 5'-GACCACTCCAATGACAACCA-3'
muGAPDH	14433	F: 5'-TTGATGGCAACAATCTCCAC-3'
		R: 5'-CGTCCCGTAGACAAAATGGT-3'
muIft88	21821	F: 5'-GCAAATGGAACGTGAAAGG-3'
		R: 5'-AAGACGCTTCGATCACAGG-3'
muKlf2	16598	F: 5'-ATTGCAACTGGGAAGGATG-3'
		R: 5'-GTGGCACTGAAAGGGTCT G-3'
muKlf4	16600	F: 5'-CAGGCGAGAAACCTTACCA-3'
		R: 5'-TGTGTGTTTGCGGTAGTGC-3'
muCdh2 (Ncad)	12558	F: 5'-AATCCCACTTATGGCCTTTC-3'
		R: 5'-AGGATTTGGGGCAAAATAAG-3'
muSerpine1 (Pai1)	18787	F: 5'-GCCAACAAGAGCCAATCAC-3'
		R: 5'-ACCCTTTCCCAGAGACCAG-3'
muSnai1	20613	F: 5'-CTTGTGTCTGCACGACCTG-3'
		R: 5'-CAGTGGGAGCAGGAGAAT-3'

Table 5.1. Sequences of the primers used for Q-PCR.
F, forward primer; R, reverse primer.

Immunohistochemistry

After deparaffination and rehydration of the sections, microwave antigen retrieval was applied by heating the slides for 12 minutes to 98ºC in citric acid buffer (0.01M in aqua-dest, pH6.0). Inhibition of endogenous peroxidase was performed after which the sections were incubated overnight with anti-phospho-Smad2 antibodies (138D4, 1:100 in PBS, Cell Signaling) and anti-αSMA antibodies (1A4, 1:3000 in 1%BSA/PBST, Sigma-Aldrich Chemie). Slides were rinsed in PBS and incubated with the secondary antibodies for 1 hour at room temperature: for phospho-Smad2 with biotin conjugated goat-anti-rabbit secondary antibodies (1:200 in PBS/1.5% NGS, Vector Laboratories) and for αSMA with horseradish peroxidase conjugated rabbit-anti-mouse antibodies (1:250 in 1%BSA/PBST, DAKO). Subsequently phospho-Smad2 stained slides were incubated with ABC-reagent (Vector Laboratories) for 45 minutes and all the slides were visualized with 400ug/ml 3-3'di-aminobenzidin tetrahydrochloride (DAB, Sigma-Aldrich Chemie). The slides were then dehydrated and mounted with Entellan (Merck). All the slides were processed simultaneously and *Tg737*$^{orpk/orpk}$ embryos (n=3) were compared with wild type littermates (n=4).

Statistical Analysis

For comparison of the means, independent experiments were performed and analyzed using SPSS 14.0 (SPSS Inc.). All results are expressed as mean ± SEM. Independent t-tests, including Levene's analyses for equality of variances, were used to analyze differences between groups. Values of $p < 0.05$ and a power ≥ 0.80 were considered statistically significant and are marked by an asterisk (*) in the figures.

Results

Shear stress induces EndoMT in nonciliated ECs

As demonstrated by immunofluorescent staining for acetylated α-tubulin, WT ECs present with primary cilia, whereas *Tg737*$^{orpk/orpk}$ ECs do not (Figure 5.1A and B). To study the effect of cilia on the response to fluid flow, WT and *Tg737*$^{orpk/orpk}$ ECs were exposed to 0.5 Pa shear stress for 24 hours. Whereas the WT ECs retained their cobblestone morphology (compare Figure 5.1C with E), nonciliated *Tg737*$^{orpk/orpk}$ ECs acquired an elongated, fibroblast-like phenotype, randomly orientated with respect to the direction of flow (compare Figure 5.1D with F). Their morphology resembled that of cells in which EndoMT was induced under static conditions with Tgfβ (Figure 5.2A). The ciliation phenotype of the ECs did not affect their capacity to undergo Tgfβ ligand–induced EndoMT, because both cell lines showed identical morphological changes. Tgfβ ligand–induced transformation of ciliated WT ECs under static conditions was characterized by loss of *CD31* expression and induction of mesenchymal markers *αSMA*, *Pai1*, *Snai1*, and *Ncad* (Figure 5.2B). Figure 5.3 summarizes the effects of shear on *Tg737*$^{orpk/orpk}$ cells. Shear-induced EndoMT was characterized by the loss of CD31 and gain of *αSMA* (Figure 5.3G). Q-PCR analysis confirmed this on the mRNA level and showed that *CD31* was downregulated by a factor of 2 and αSMA was induced 26-fold under shear stress, compared to the static controls (Figure 5.3A and B). *Pai1*, which is a downstream activation marker of the type I Tgfβ receptor Alk5, was induced 56-fold under shear (Figure 5.3C). *Snai1*, a downstream target of Tgfβ and a marker for EndoMT, and *Ncad*, a transmembrane protein characteristic for mesenchymal cells, were both significantly induced by shear stress in *Tg737*$^{orpk/orpk}$ cells (Figure 5.3D and E). In comparison, ciliated WT ECs did not show altered *CD31* expression under fluid flow; showed only a slight induction of *αSMA*, *Pai1*, and *Snai1*; and did not induce *Ncad* (Figure 5.3A through E). Indeed, the majority of WT cells were still ciliated under these conditions (Figure 5.4A). To study the effect of magnitude of shear on ciliation phenotype of ECs and their concomitant response to fluid flow, WT and *Tg737*$^{orpk/orpk}$ ECs were exposed to 2.5 Pa shear stress for 24 hours. WT ECs became nonciliated and underwent EndoMT similar to that observed in *Tg737*$^{orpk/orpk}$ cells (Figure 5.4A). These morphological changes were reflected by expression changes of *CD31*, *αSMA*, *Pai1*, *Snai1*, and *Ncad* (Figure 5.4B).

EndoMT is Tgfβ/Alk5 kinase–dependent

The role of Tgfβ/Alk5 signaling in shear stress–induced EndoMT was investigated using flow in the presence of either a pan-Tgfβ neutralizing antibody (α-Tgfβ) or the Alk5 kinase inhibitor compound SB431542. Depletion of Tgfβ ligand from the culture medium by binding to α-Tgfβ, as well as inhibiting Alk5 kinase activity, prevented EndoMT under shear stress in *Tg737*$^{orpk/orpk}$ ECs (Figure 5.3A through F and H). This was marked by the retention of cobblestone morphology (Figure 5.3H) and CD31 expression and by the lack of αSMA induction (not shown). After shear stress in the presence of α-Tgfβ, *Pai1* induction was reduced from 56- to 18-fold, and expression of *Snai1*, *αSMA*, *Ncad*, and *CD31* remained unchanged compared to the static controls (Figure 5.3A through E).

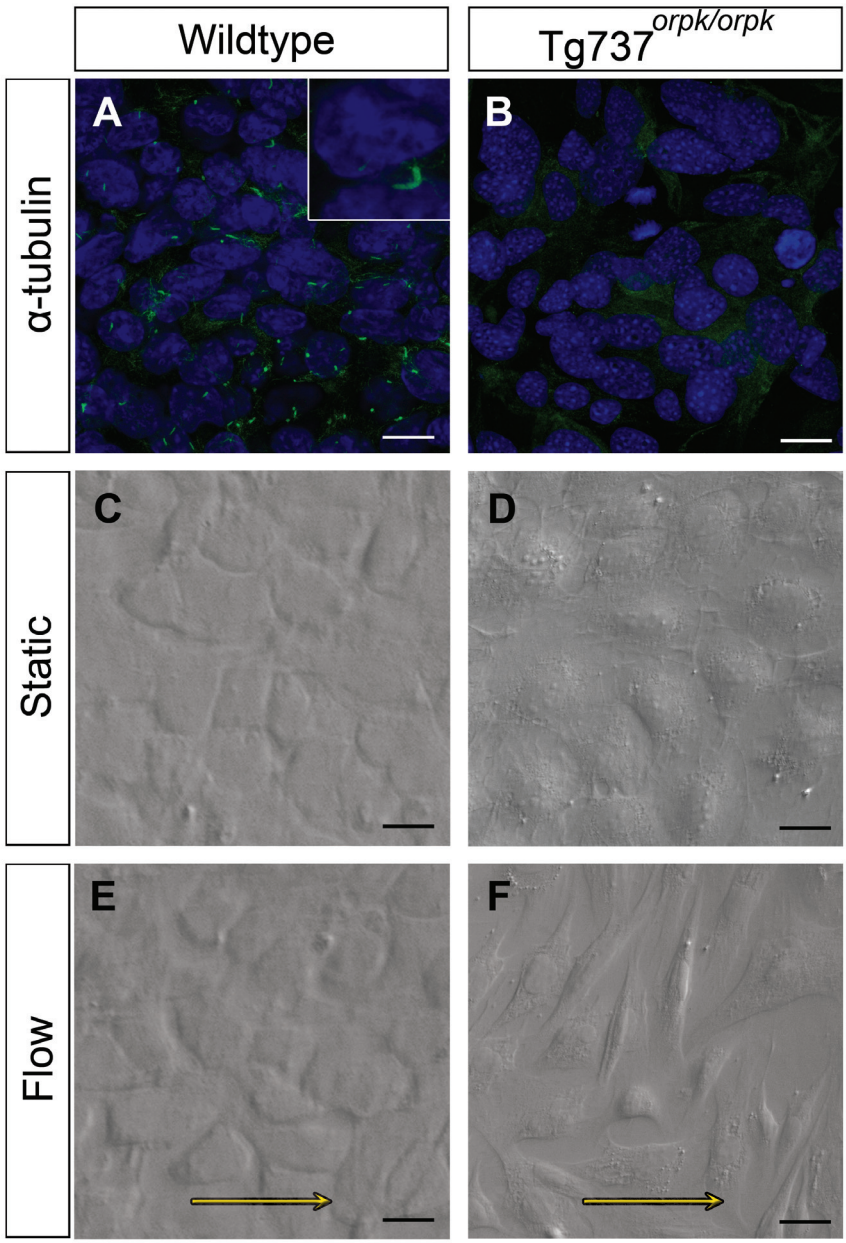

Figure 5.1. Different responses to shear stress of ciliated and nonciliated ECs. A and B, Immunostaining for acetylated-tubulin showing the presence of cilia in WT ECs and absence of cilia in *Tg737*$^{orpk/orpk}$ ECs. C and D, WT and *Tg737*$^{orpk/orpk}$ ECs show a cobblestone morphology under static conditions. E and F, WT ECs retain their phenotype under flow, whereas *Tg737*$^{orpk/orpk}$ ECs undergo EndoMT. Arrows indicate the direction of flow. Scale bars: 35μm (A and B); 25μm (C through F).

The response to shear stress in the presence of the SB compound largely mimicked the response in the presence of α-Tgfβ. *Pai1* induction under flow was reduced to 26-fold; *Snai1*, *αSMA*, and *Ncad* expression was no longer induced (Figure 5.3B through E). *CD31* mRNA expression was induced under these conditions, but this was not reflected on protein level (Figure 5.3A and F). Tgfβ-induced Alk5 kinase activation, and induction of the downstream signaling pathways therefore plays a critical role in the shear stress response and in EndoMT.

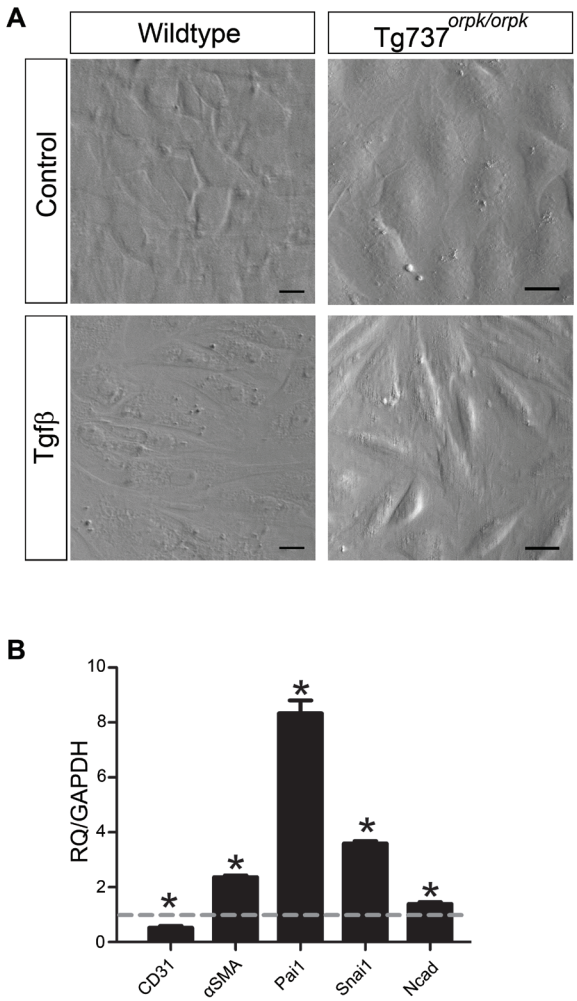

Figure 5.2. Tgfβ induced EndoMT in ciliated WT and non-ciliated *Tg737*$^{orpk/orpk}$ ECs. A, Morphology of WT and *Tg737*$^{orpk/orpk}$ cells which were stimulated with Tgfβ ligand to induce EndoMT under static conditions. Note the transition from cobble-stone to fibroblast-like morphology upon stimulation with Tgfβ. Scale bars: 25μm. B, Relative mRNA expression of *CD31*, *αSMA*, *Pai1*, *Snai1*, and *Ncad* in WT ECs upon stimulation with Tgfβ ligand. Expression is normalized to *GAPDH* and relative to shams, as represented by the dashed line.

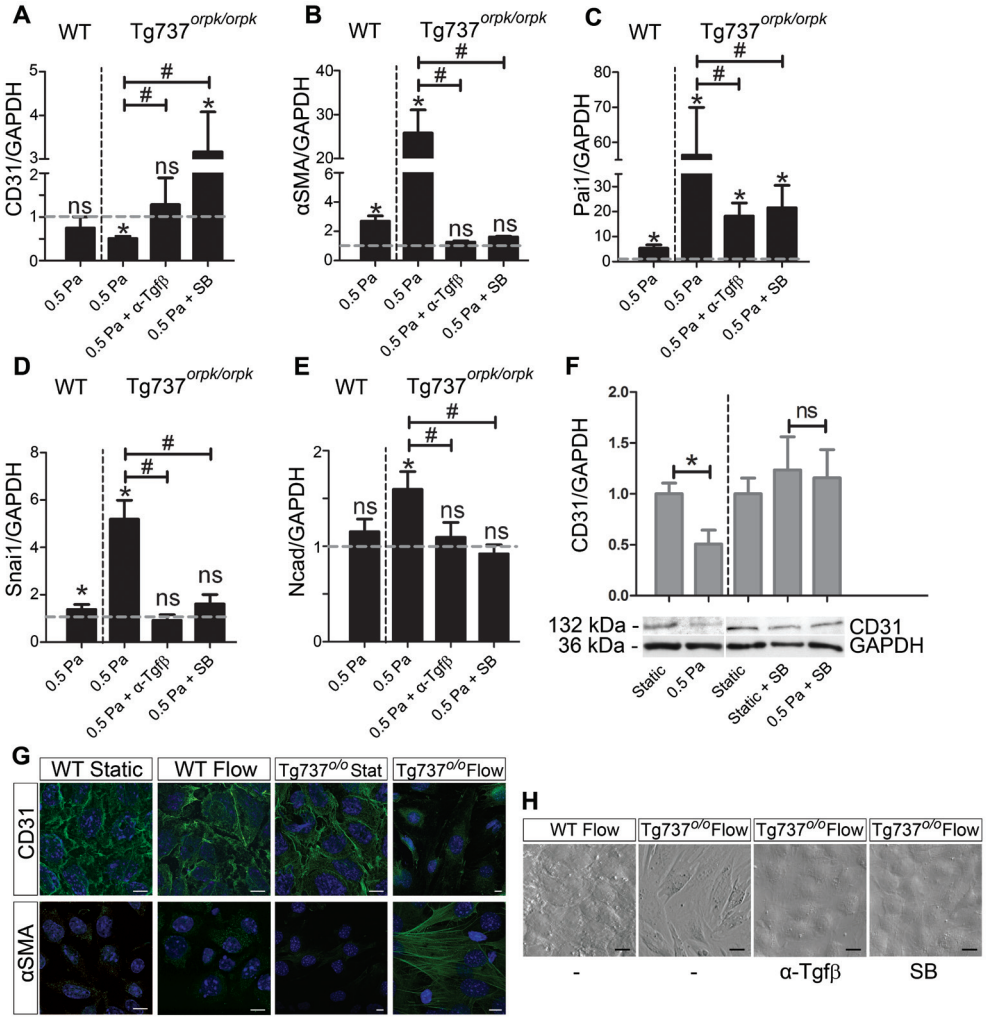

Figure 5.3. Shear stress–induced EndoMT in nonciliated ECs is Tgfβ/Alk5-dependent. A through E, Relative mRNA expression of *CD31*, *αSMA*, *Pai1*, *Snai1*, and *Ncad* in WT and *Tg737*$^{orpk/orpk}$ cells under 0.5 Pa shear with and without pan-Tgfβ neutralizing antibody (α-Tgfβ) and SB431542 (SB). Expression is normalized to *GAPDH* and relative to static shams, as represented by the dashed line. F, Western blot analysis and quantification of CD31 protein levels in *Tg737*$^{orpk/orpk}$ cells under static conditions, and under 0.5 Pa shear stress with and without SB. G, CD31 and αSMA immunostainings of WT and *Tg737*$^{orpk/orpk}$ ECs under static conditions and after exposure to 0.5 Pa shear stress. Scale bars: 25 μm. H, Morphology of WT and *Tg737*$^{orpk/orpk}$ cells under 0.5 Pa shear with and without α-Tgfβ and SB. Scale bars: 25 μm.

Role of cilia in defining the Klf2/Klf4 response to shear stress

The specific response of WT and *Tg737*$^{orpk/orpk}$ ECs to shear stress was investigated by analyzing the expression levels of *Klf2* and *Klf4* after exposure to 0.5 Pa shear for 24 hours. WT ECs showed a 2.3- and 1.8-fold induction of *Klf2* and *Klf4*, respectively, whereas *Tg737*$^{orpk/orpk}$ cells failed to induce *Klf2* (Figure 5.5A and B). Remarkably, the latter cells showed a marked downregulation of *Klf4* by more than 75% under shear stress (Figure 5.5B). In *Tg737*$^{orpk/orpk}$ cells, shear stress–related upregulation of *Klf2* was restored and downregulation of *Klf4* was prevented when Tgfβ signaling was inhibited with the SB compound or in the presence of α-Tgfβ (Figure 5.5A and B). The responses of *Klf4* mRNA were accurately reflected at the protein level (Figure 5.5C).

Klf4 overexpression prevents shear stress–induced EndoMT

To investigate whether shear-induced EndoMT in *Tg737*$^{orpk/orpk}$ cells was a result of the marked downregulation of Klf4 or is rather the cause of it, Klf4 was transiently overexpressed (*Tg737*$^{orpk/orpk}$*-Klf4*) and transfected cells were exposed to 0.5 Pa shear stress for 24 hours. *Tg737*$^{orpk/orpk}$ with LacZ overexpression (*Tg737*$^{orpk/orpk}$*-LacZ*) were used as a control. *Tg737*$^{orpk/orpk}$*-Klf4* showed a 10-fold overexpression of *Klf4* mRNA, an effect that was confirmed at the protein level (Figure 5.6A and B). Under shear stress, *Tg737*$^{orpk/orpk}$*-Klf4* ECs retained their cobblestone morphology, CD31 expression, and did not undergo EndoMT (Figure 5.6C through E). *Pai1* induction was reduced from 34- to 9-fold, *Snai1* was induced only 1.9-fold, compared to 3.2-fold in the control group, and *Ncad* was not induced under flow (Figure 5.6D). Overexpression of Klf4 did not result in the reappearance of the cilium (not shown), demonstrating that prevention of flow induced EndoMT in *Tg737*$^{orpk/orpk}$*-Klf4* was not a secondary effect of ciliary rescue.

Rescue of cilia prevents shear stress–induced transdifferentiation of ECs

Tg737$^{orpk/orpk}$ ECs were stably transfected with Ift88-mCherry cDNA to generate *Tg737*$^{orpk/orpk}$*–Ift88**. Figure 5.7A and B shows that Ift88 mRNA and Ift88* protein levels in rescued cells were comparable to the Ift88 levels in WT ECs. Rescue of Ift88 in *Tg737*$^{orpk/orpk}$ ECs led to a structural rescue of the cilia, with a normal distribution of one primary cilium per single cell (Figure 5.7C). To confirm functional rescue, *Tg737*$^{orpk/orpk}$*–Ift88** cells were subjected to 0.5 Pa shear stress for 24 hours, a condition that induced EndoMT in nonrescued cells. Cells now retained their cobblestone morphology and did not undergo EndoMT (Figure 5.7D). Q-PCR analysis showed induction of *Pai1* and *αSMA* similar in magnitude to that of the WT ECs under shear, without any changes in the expression levels of *CD31*, *Snai1*, and *Ncad* (Figure 5.7E). The table in Figure 5.7E shows the ratios of relative (to static controls) expression levels of genes of interest in *Tg737*$^{orpk/orpk}$*–Ift88**, compared to WT ECs under shear. The expression profiles of these two cell types under shear stress are comparable and rescue of the cilia led to induction of *Klf2* and lack of *Klf4* downregulation under flow.

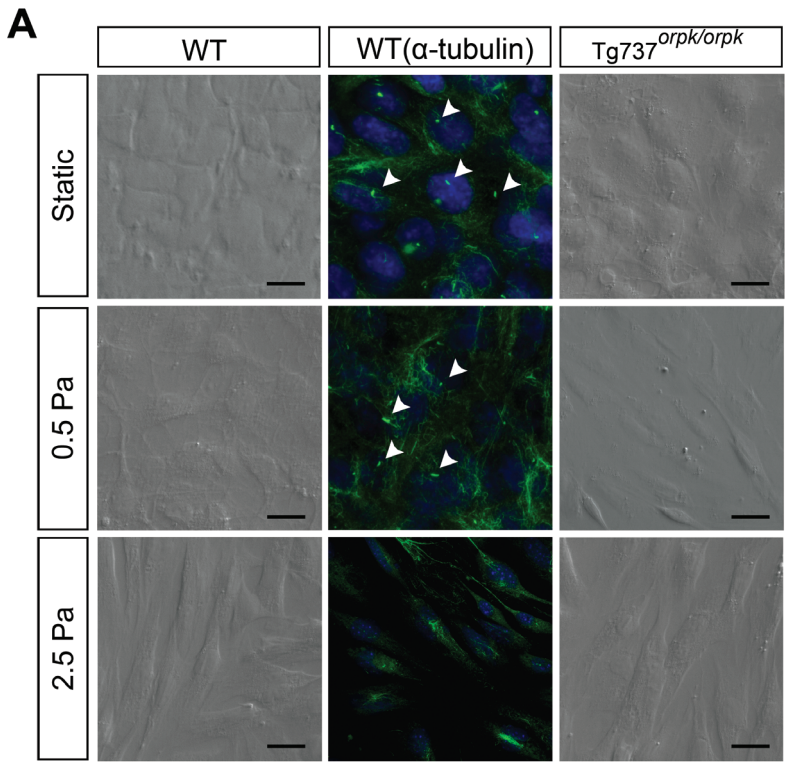
A
WT
WT(α-tubulin)
Tg737orpk/orpk
Static
0.5 Pa
2.5 Pa

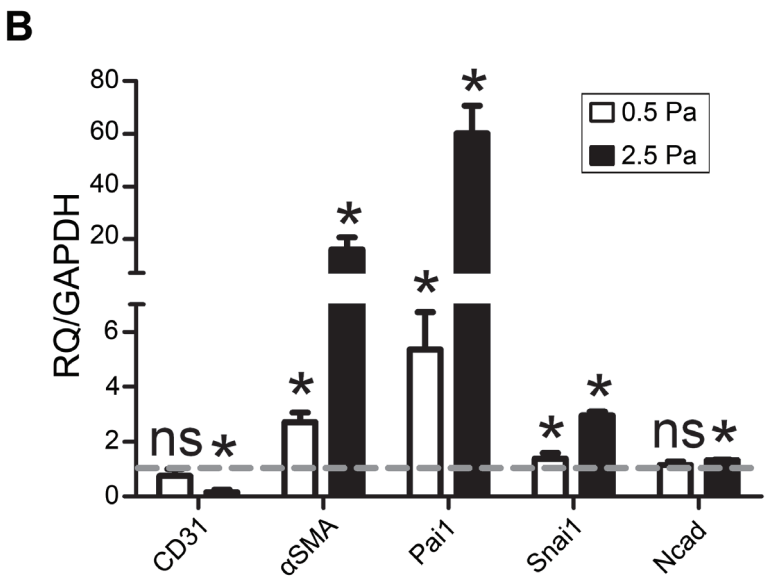
B
RQ/GAPDH
80
60
40
20
6
4
2
0
0.5 Pa
2.5 Pa
ns
*
CD31
αSMA
Pai1
Snai1
Ncad

◄ Figure 5.4. **WT ECs loose their cilia and undergo EndoMT after exposure to high flow.** A, Morphology of WT (left and middle column) and *Tg737*$^{orpk/orpk}$ cells (right column) under static conditions (top row) and after exposure to 0.5 and 2.5 Pa shear stress (middle and lower rows, respectively). The central column shows immunostaining for acetylated α-tubulin. Arrowheads indicate cilia. Note the presence of primary cilia at 0.5 Pa shear and the non-ciliated phenotype of WT cells after exposure to 2.5 Pa shear stress. Scale bars: 25µm. B, Relative mRNA expression of *CD31*, *αSMA*, *Pai1*, *Snai1*, and *Ncad* in WT cells under 0.5 and 2.5 Pa shear. Expression is normalized to *GAPDH* and relative to static shams, as represented by dashed line.

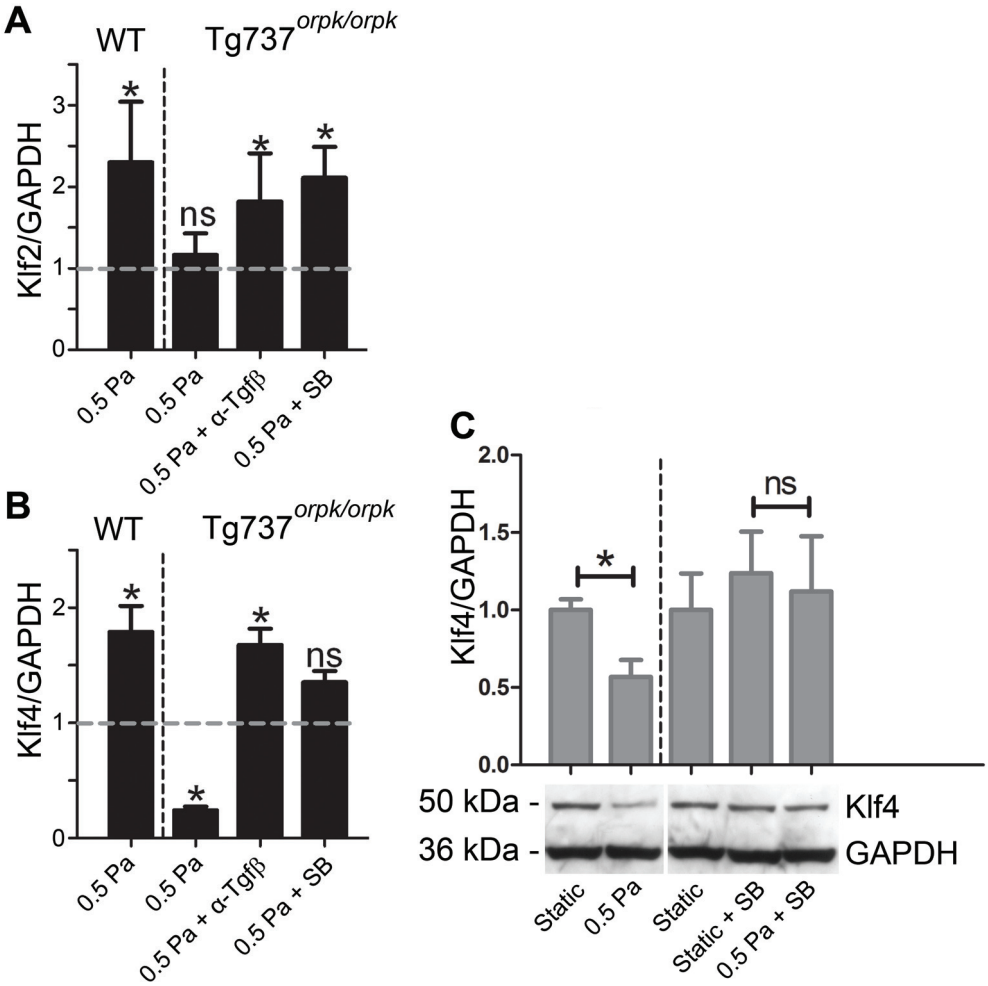

Figure 5.5. **Klf2 and Klf4 response of WT and Tg737**$^{orpk/orpk}$ **ECs to shear stress.** A and B, Relative mRNA expression of *Klf2* and *Klf4* in WT and *Tg737*$^{orpk/orpk}$ cells under 0.5 Pa shear stress with and without pan-Tgfβ neutralizing antibody (α-Tgfβ) and SB431542 (SB). Expression is normalized to *GAPDH* and relative to static shams, as represented by the dashed line. C, Western blot analysis and quantification of Klf4 protein levels in *Tg737*$^{orpk/orpk}$ cells under static conditions, and under 0.5 Pa shear stress with and without SB431542.

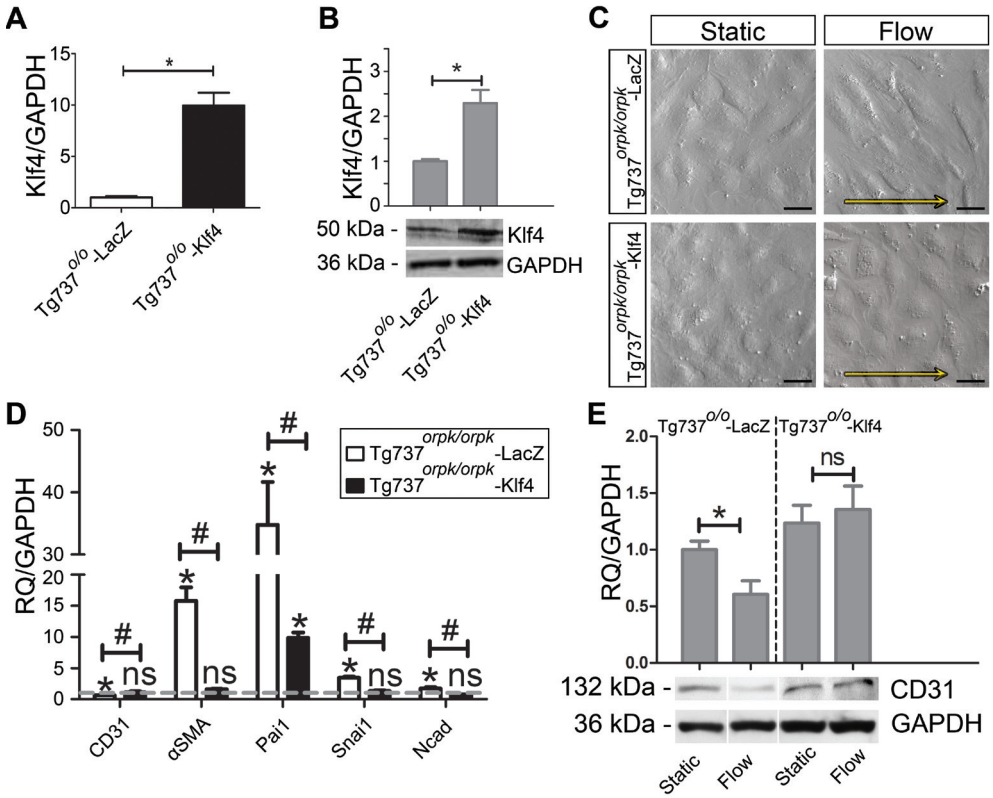

Figure 5.6. Klf4 overexpression prevents shear stress–induced EndoMT. A and B, Q-PCR and Western blot analysis, respectively, showing Klf4 overexpression in *Tg737*$^{orpk/orpk}$ ECs that were transfected with either LacZ (*Tg737*$^{o/o}$*-LacZ*, sham) or Klf4 (*Tg737*$^{o/o}$*-Klf4*) expression constructs. Transfection with Klf4 results in a 10-fold overexpression on mRNA level and a 2.2-fold overexpression on protein level. C, Images of *Tg737*$^{orpk/orpk}$*-LacZ* and *Tg737*$^{orpk/orpk}$*-Klf4* cells under static conditions and under 0.5 Pa shear stress. Arrows indicate the direction of flow. Scale bars: 25 µm. D, Q-PCR showing relative mRNA expression of *CD31*, *αSMA*, *Pai1*, *Snai1*, and *Ncad* in *Tg737*$^{orpk/orpk}$*-LacZ* and *Tg737*$^{orpk/orpk}$*-Klf4* cells under 0.5 Pa shear stress. Expression is normalized to *GAPDH* and relative to static shams, as represented by the dashed line. E, Western blot analysis and quantification of CD31 protein in *Tg737*$^{orpk/orpk}$*-LacZ* and *Tg737*$^{orpk/orpk}$*-Klf4* cells under static conditions and 0.5 Pa shear stress.

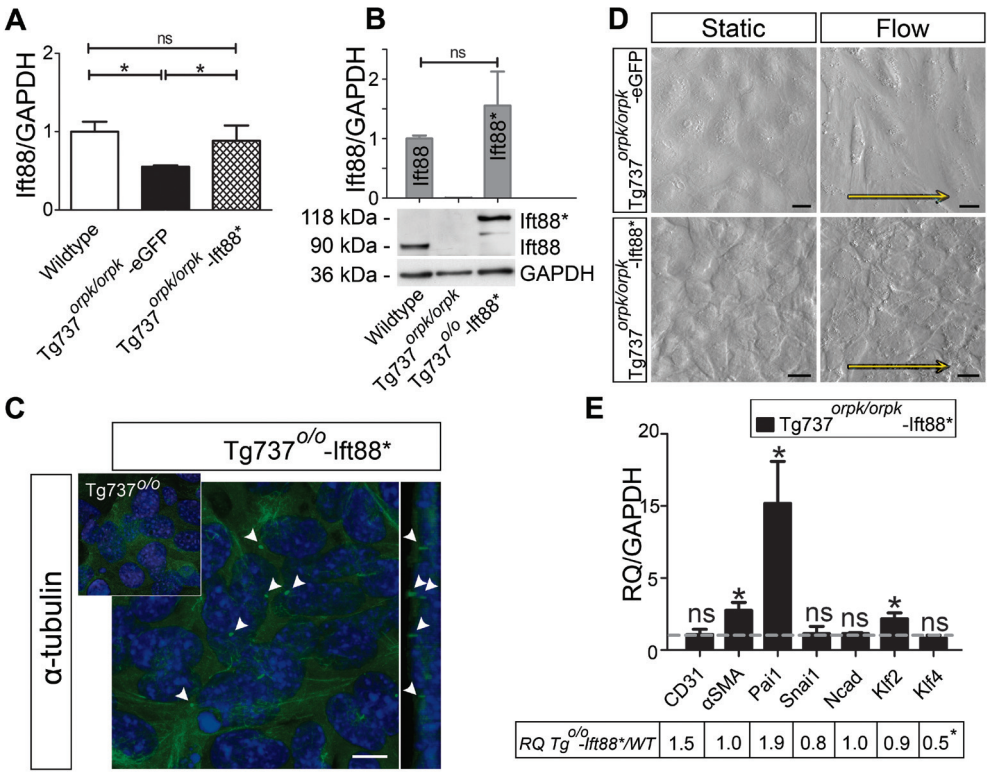

Figure 5.7. Rescue of Ift88 leads to functional rescue of the cilia and prevents shear stress–induced EndoMT in *Tg737*$^{orpk/orpk}$ ECs. A and B, Q-PCR and Western blot analysis, respectively, showing Ift88 levels in WT and *Tg737*$^{orpk/orpk}$ stably transfected with pEGFP-N1 (*Tg737*$^{o/o}$*-eGFP*, sham) and Ift88-mCherry/Ift88* (*Tg737*$^{o/o}$*-Ift88**) expression constructs. Transfection with Ift88* results in a 2-fold increase in mRNA level of *Ift88** in *Tg737*$^{orpk/orpk}$ ECs and normalizes protein levels to those of Ift88 in WT ECs. C, Confocal images with optical cross section of *Tg737*$^{orpk/orpk}$ cells, immunostained for acetylated tubulin, showing the presence of cilia in rescued *Tg737*$^{orpk/orpk}$*-Ift88** ECs but not in nonrescued cells (inset). Arrowheads point toward primary cilia and scale bar represents 10 µm. D, Images of *Tg737*$^{orpk/orpk}$*-Ift88** cells under static conditions and under 0.5 Pa shear stress. Arrows indicate the direction of flow and scale bars represent 25 µm. E, Q-PCR showing relative mRNA expression of *CD31*, αSMA, *Pai1*, *Snai1*, *Ncad*, *Klf2*, and *Klf4* in *Tg737*$^{orpk/orpk}$*-Ift88** cells under 0.5 Pa shear stress. Expression is normalized to *GAPDH* and relative to static shams, as represented by the dashed line. The table shows the ratios of relative mRNA expression levels of *Tg737*$^{orpk/orpk}$*–Ift88** and WT ECs under shear stress.

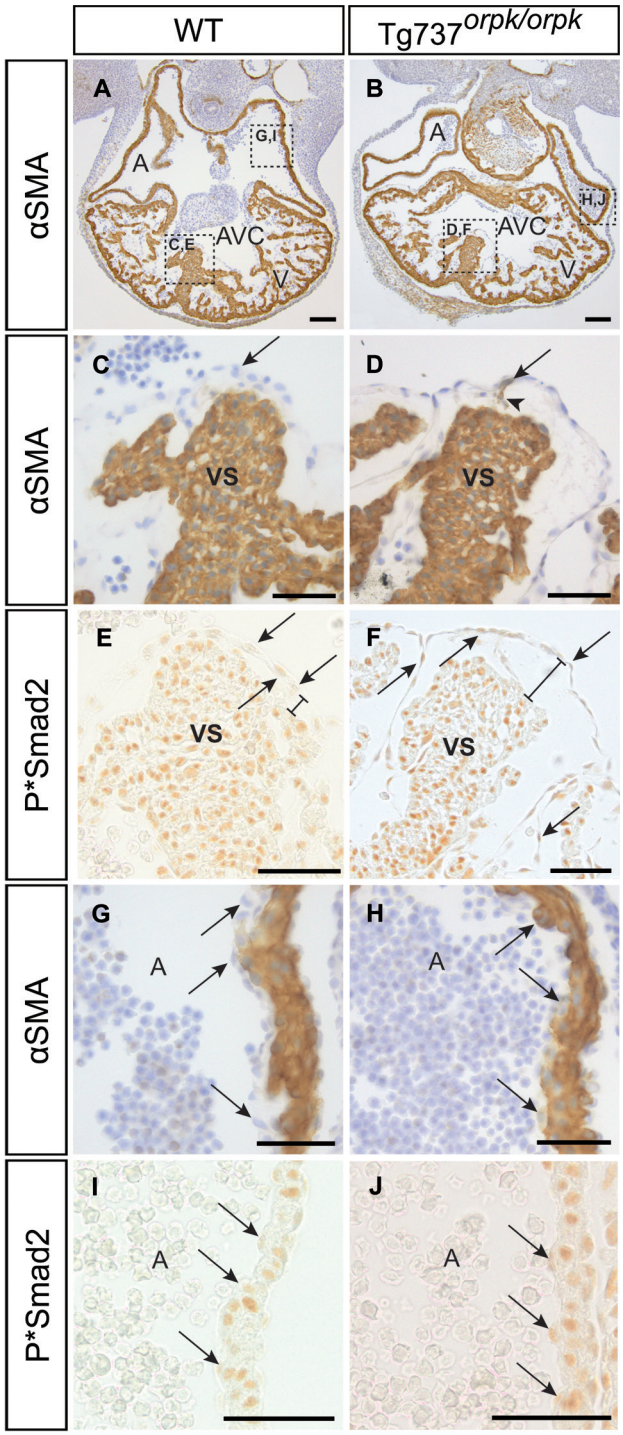

Figure 5.8. Lack of cilia primes ECs for shear-induced activation of Tgfβ signaling, *in vivo*. Transverse sections through the hearts of WT (A, C, E, G, and I) and *Tg737*$^{orpk/orpk}$ (B, D, F, H, and J) mouse embryos of stage E11.5 comparing the expression of αSMA and phosphorylated Smad2 (P*Smad2). Boxed areas in A and B are magnified in C through J in these or adjacent sections. αSMA-positive cells are observed in the endothelium of the ventricular septum and trabeculations of *Tg737*$^{orpk/orpk}$ embryos (compare C with D). The ECs of *Tg737*$^{orpk/orpk}$ embryos have higher expression of P*Smad2 compared to WT littermates (compare E with F). The subendothelial space of the ventricular septum and trabeculations, representing cardiac jelly, is increased in the mutants (compare C and E with D and F). The atria of WT animals are lined by ECs negative for αSMA and P*Smad2, whereas these cells stain positive for both markers in the *Tg737*$^{orpk/orpk}$ embryos (compared G and I with H and J). A indicates atrium; AVC, atrioventricular canal; V, ventricle; VS, ventricular septum. Scale bars: 100 μm (A and B); 50 μm (C through J).

Nonciliated ECs activate Tgfβ signaling *in vivo*

To assess the *in vivo* consequences of (non)ciliation of ECs for Tgfβ/Alk5 signaling activation, the hearts of embryonic day (E)11.5 WT and *Tg737*$^{orpk/orpk}$ mouse embryos were analyzed for endothelial expression of phosphorylated Smad2 (P*Smad2) and αSMA (Figure 5.8). ECs of *Tg737*$^{orpk/orpk}$ embryos lining areas of low shear (ie, in the atria, on the ventricular septum, and on trabeculations) show increased expression of P*Smad2 compared to their WT littermates, pointing toward enhanced Tgfβ/Alk5 activation. *Tg737*$^{orpk/orpk}$ embryos also have αSMA-positive cells in these areas, whereas all ECs in the WT embryos were negative for αSMA. Moreover, the subendocardial space of the ventricular septum and trabeculations is increased in the mutant embryos, suggesting increased extracellular matrix production and deposition. Western blot analysis of P*Smad2 levels in WT and *Tg737*$^{orpk/orpk}$ ECs after exposure to 2 hours of shear stress showed an increase of P*Smad2 levels by 30% in the WT ECs, compared to a 2.2-fold increase in the *Tg737*$^{orpk/orpk}$ cells, confirming enhanced P*Smad2 signaling in nonciliated cells (Figure 5.9).

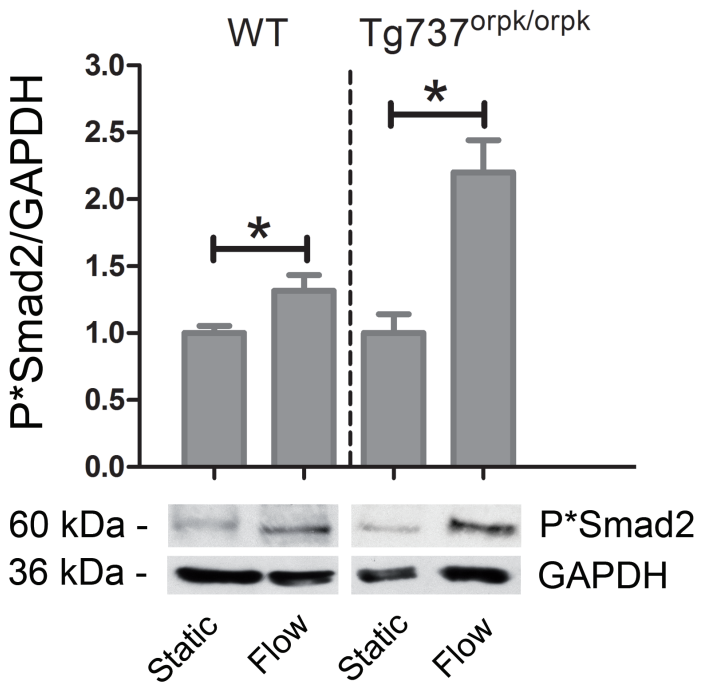

Figure 5.9. Exposure to shear stress results in enhanced phospho-Smad2 expression in *Tg737*$^{orpk/orpk}$ cells. Western Blot analysis and quantification of P*Smad2 protein levels in WT and *Tg737*$^{orpk/orpk}$ cells under static conditions and after exposure to 2 hours of 0.5 Pa shear stress. Western Blot shown is representative of 3 independent experiments.

Discussion

In this study, we used ECs deficient in functional Ift88 protein[34] and thus lacking the ability to form cilia. They provide a robust model to analyze the functional role of primary cilia in response to fluid flow. Although the effects of ciliary dysfunction on kidney epithelial cells and their response to flow has been the subject of numerous studies, the effects of dysfunctional primary cilia on ECs remain largely unknown. *In vivo* EC primary cilia are present in areas of low and disturbed shear stress[17,19], where they have been suggested to play an important role in mechanosensing[10]. In our model, ciliated ECs retained an endothelial phenotype in response to 0.5 Pa shear stress *in vitro*, whereas nonciliated *Tg737*$^{orpk/orpk}$ ECs underwent EndoMT and adopted a fibroblast-like phenotype. When exposed to higher shear levels, which resulted in the deciliation of WT ECs, these cells also underwent EndoMT and gained a phenotype that closely resembled that of *Tg737*$^{orpk/orpk}$ ECs under flow. It is therefore plausible that WT ECs disassemble their cilia under high laminar shear stress, as has previously been reported for chicken and human ECs[17,35], priming the cells for shearinduced EndoMT. In this respect, shear-induced EndoMT of nonciliated cells should be clearly distinguished from flowinduced endothelial alignment, which has been described extensively. Here, the direction of cellular elongation was random with respect to the direction of flow, and the changes in phenotype were accompanied by the loss of endothelial markers and the gain of mesenchymal and transition markers. ECs of various origins have been demonstrated to undergo EndoMT *in vitro* when exposed to Tgfβ[26]. We confirmed these findings in the WT and *Tg737*$^{orpk/orpk}$ ECs and identified Tgfβ/Alk5 kinase activity to be essential in shear stress–mediated EndoMT. Because treatment with either Tgfβ blocking antibodies or Alk5 kinase inhibitor prevented shear-induced transformation, an autocrine mechanism by which flow activates Tgfβ production or promotes its bioavailability, which, in turn, activates signaling by binding to its receptors on ECs, appears feasible. However, this requires further confirmation.

A typical response of endothelial cells to shear stress is upregulation of the zinc finger transcription factor KLF2. *In vivo*, expression of KLF2 in the embryonic and adult cardiovascular system is confined to areas of high shear stress[20,36]. *In vitro*, KLF2 is induced by flow[21,37] and acts as a regulator of endothelial function through regulation of multiple genes[14,36]. Here, we confirm the shear-dependent upregulation of Klf2 in ciliated ECs but also show that the absence of cilia in *Tg737*$^{orpk/orpk}$ cells prevents this induction. This is in line with previous results showing attenuation of KLF2 induction in deciliated chicken ECs[10]. Like KLF2, KLF4 has been reported to be expressed in ECs in a shear-dependent manner[38]. Ciliated ECs show a similar response in our experimental setting. Nonciliated cells, however, show a dramatic downregulation of this transcription factor. We show that this downregulation of Klf4 not only coincides with EndoMT but is, in fact, required for this transition. Preventing downregulation by artificial overexpression of Klf4 or by blocking Tgfβ signaling also prevents shear stress–induced EndoMT, as demonstrated by the retention of CD31

expression and a cobblestone phenotype, and by the lack of induction of transition markers like *αSMA*, *Pai1*, *Snail*, and *Ncad*. This is in line with studies that show that Klf4 potently represses the expression of smooth muscle differentiation markers, including αSMA[39], in vascular smooth muscle cells and is rapidly induced following vascular injury[40]. Smooth muscle differentiation also largely depends on Tgfβ signaling[39] and probably involves a similar transition mechanism.

To ensure that the differences in response to shear stress and the process of EndoMT were specific to the lack of cilia on ECs, Ift88 was stably overexpressed in *Tg737*$^{orpk/orpk}$ cells. This resulted in the reappearance of primary cilia in a normal distribution pattern of one per cell. *Tg737*$^{orpk/orpk}$*–Ift88** ECs responded to shear stress in a manner similar to the WT ECs, reflected by the induction of *Klf2*, lack of downregulation of Klf4, and the retention of an endothelial phenotype under flow. This identifies the primary cilium as a necessary element to retain endothelial quiescence under low flow conditions. Together, this confirms the central role of primary cilia in defining a functional response to fluid flow in ECs, as is illustrated in Figure 5.10. In short, ciliated ECs retain their cobblestone morphology under shear stress, whereas nonciliated ECs undergo flow mediated EndoMT. This transition is preceded by the activation of Tgfβ/Alk5 signaling and downregulation of transcription factor Klf4. Shear stress–induced EndoMT in nonciliated cells can be prevented in vitro by interfering with Tgfβ signaling, by rescuing the cilium, or by induction of Klf4 expression.

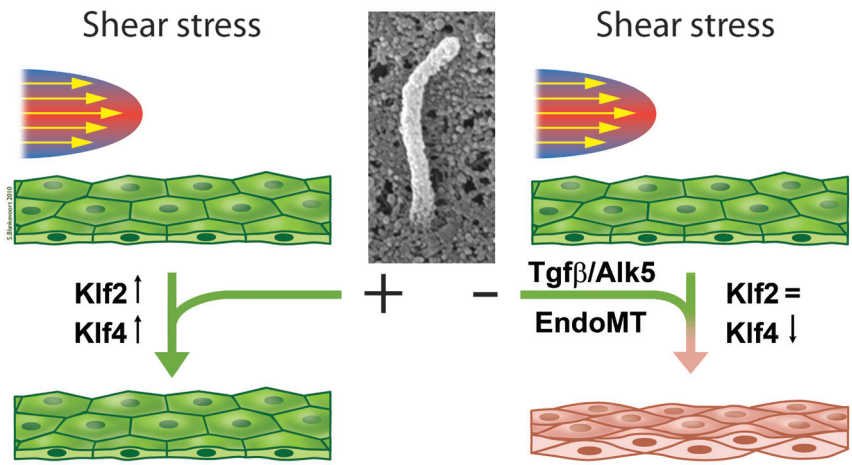

Figure 5.10. **Model for the role of primary cilia in shear response of ECs.** Depending on the flow pattern, ECs can be ciliated or not. The center picture shows a scanning electron micrograph of an endothelial cilium. When ciliated ECs (+) are exposed to shear stress they show induction of Klf2 and Klf4 and retain a cobblestone endothelial phenotype (green arrow). However, when nonciliated cells (-) are exposed to flow, they fail to induce Klf2 and downregulate Klf4. They lose their endothelial characteristics and acquire a mesenchymal or transition phenotype (red arrow/cells) in a Tgfβ/Alk5-dependent manner. This potentially pathological transition can be prevented by eg, blocking Tgfβ signaling or by inducing Klf4 expression.

Our *in vivo* data confirm the relation between the absence of primary cilia and activation of Tgfβ signaling. In the hearts of *Tg737*$^{orpk/orpk}$ embryos, ECs that would normally be ciliated[17,18] now showed increased Smad2 phosphorylation and αSMA expression, indicating activation of Tgfβ signaling. This is supported by increased production of extracellular matrix, resulting in more cardiac jelly, as observed in the *Tg737*$^{orpk/orpk}$ embryos. However, these embryos did not show concomitant excessive EndoMT in the low-flow areas. Apparently, other factors, most probably locally secreted by the myocardium, inhibit the final transition into mesenchymal cells in these embryos. This is in line with previous studies that suggest an EndoMT-stimulatory environment, specifically in the atrioventricular canal and outflow tract of the embryonic heart, resulting from paracrine signaling. As a consequence of the high levels of shear stress[20,22,41–44], the ECs in these areas are already nonciliated during cushion EndoMT stages in WT embryos, and altered EndoMT attributable to lack of cilia in *Tg737*$^{orpk/orpk}$ mice was not expected. Indeed, in the *Tg737*$^{orpk/orpk}$ embryos, no abnormalities with respect to Tgfβ activation patterns in areas of high shear or cushion development were identified. Whether cilia and altered flow–induced EndoMT play a role under pathological conditions in adult mutant mice, such as atherosclerosis or heart failure–related cardiac fibrosis[45], will need to be determined in future studies.

Appreciation for ciliary function in development and normal human physiology has led to reanalysis of a number of human syndromes that have previously been associated merely on the basis of similar clinical features. Several ciliopathies are characterized by gross cardiac anomalies, probably related to the failed orientation of heart looping along the left–right axis, corresponding to the high incidence of situs inversus in these patients[2,46,47]. Here, we provide data to suggest that ECs might contribute to the phenotypes observed in these syndromes; in which case, their defects in the cardiovascular system could be masked by the gross anomalies of disturbed left-right asymmetry. Studies have shown mice with mutations leading to complete loss of cilia or defective mechanosensation to have 100% penetrance of intracardiac defects, next to the prominent left–right patterning abnormalities[2,48]. In contrast, only ≈ 40% of mice with structurally normal, but immotile, cilia have intracardiac defects that are mostly associated with abnormal left–right development[49]. These observations lead to the belief that cilia have a broader role in heart development than through their function in node cilia alone[18]. Furthermore, endothelial dysfunction and increased carotid intima–media thickness has been reported with increased frequency in adult polycystic kidney disease patients[50], pointing toward a role for cilia in vascular function.

Acknowledgments

We thank Venus C. Roper (University of Alabama at Birmingham Department of Cell Biology) for harvesting the embryos and Emile de Heer and Wim Corver (LUMC Department of Pathology) for generously providing the antibodies. Sebastiaan Blankevoort (LUMC Department of Anatomy and Embryology) is acknowledged for preparation of the artwork in Figure 5.10. Christine L. Mummery (LUMC Department of Anatomy and Embryology) is gratefully acknowledged for help with the manuscript.

Surya M. Nauli is supported by grant DK080640. Bradley K. Yoder is supported by NIH P30 DK074038 Hepato/Renal Fibrocystic Diseases Core Center and Peter ten Dijke by the Leducq Foundation and Centre for Biomedical Genetics.

References

1. D'Angelo A, Franco B. The dynamic cilium in human diseases. *Pathogenetics*. 2009;2(1):3.
2. Nonaka S, Tanaka Y, Okada Y, Takeda S, Harada A, Kanai Y, Kido M, Hirokawa N. Randomization of left-right asymmetry due to loss of nodal cilia generating leftward flow of extraembryonic fluid in mice lacking KIF3B motor protein. *Cell*. 1998;95:829-837.
3. Satir P, Christensen ST. Overview of Structure and Function of Mammalian Cilia. *Annu Rev Physiol*. 2007;69:377-400.
4. Baker K, Beales PL. Making sense of cilia in disease: the human ciliopathies. *Am J Med Genet C Semin Med Genet*. 2009;151C:281-295.
5. Rosenbaum JL, Witman GB. Intraflagellar transport. *Nature Reviews Molecular Cell Biology*. 2002;3:813-825.
6. Singla V, Reiter JF. The primary cilium as the cell's antenna: signaling at a sensory organelle. *Science*. 2006;313:629-633.
7. Goldsmith HL, Cokelet GR, Gaehtgens P. Robin Fahraeus: evolution of his concepts in cardiovascular physiology. *Am J Physiol*. 1989;257:H1005-H1015.
8. Praetorius HA, Spring KR. Removal of the MDCK cell primary cilium abolishes flow sensing. *J Membr Biol*. 2003;191:69-76.
9. Nauli SM, Kawanabe Y, Kaminski JJ, Pearce WJ, Ingber DE, Zhou J. Endothelial cilia are fluid-shear sensors that regulate calcium signaling and nitric oxide production through polycystin-1. *Circulation*. 2008;117:1161-1171.
10. Hierck BP, Van der Heiden K, Alkemade FE, van de Pas S, van Thienen JV, Groenendijk BCW, Bax WH, Van der Laarse A, DeRuiter MC, Horrevoets AJG, Poelmann RE. Primary Cilia Sensitize Endothelial Cells for Fluid Shear Stress. *Dev Dyn*. 2008;237:725-735.
11. Nauli SM, Alenghat FJ, Luo Y, Williams E, Vassilev P, Lil XG, Elia AEH, Lu WN, Brown EM, Quinn SJ, Ingber DE, Zhou J. Polycystins 1 and 2 mediate mechanosensation in the primary cilium of kidney cells. *Nature Genetics*. 2003;33:129-137.
12. Poelmann RE, Van der Heiden K, Gittenberger-de Groot AC, Hierck BP. Deciphering the endothelial shear stress sensor. *Circulation*. 2008;117:1124-1126.
13. Parmar KM, Larman HB, Dai G, Zhang Y, Wang ET, Moorthy SN, Kratz JR, Lin Z, Jain MK, Gimbrone MA, Garcia-Cardena G. Integration of flow-dependent endothelial phenotypes by Krüppel-like factor 2. *J Clin Invest*. 2006;116:49-58.
14. Dekker RJ, Boon RA, Rondaij MG, Kragt A, Volger OL, Elderkamp YW, Meijers JC, Voorberg J, Pannekoek H, Horrevoets AJG. KLF2 provokes a gene expression pattern that establishes functional quiescent differentiation of the endothelium. *Blood*. 2006;107:4354-4363.
15. Hamik A, Lin Z, Kumar A, Balcells M, Sinha S, Katz J, Feinberg MW, Gerzsten RE, Edelman ER, Jain MK. Krüppel-like factor 4 regulates endothelial inflammation. *J Biol Chem*. 2007;282:13769-13779.
16. Villarreal G, Jr., Zhang Y, Larman HB, Gracia-Sancho J, Koo A, Garcia-Cardena G. Defining the regulation of KLF4 expression and its downstream transcriptional targets in vascular endothelial cells. *Biochem Biophys Res Commun*. 2010;391:984-989.
17. Van der Heiden K, Groenendijk BCW, Hierck BP, Hogers B, Koerten HK, Mommaas AM, Gittenberger-de Groot AC, Poelmann RE. Monocilia on chicken embryonic endocardium in low shear stress areas. *Dev Dyn*. 2006;235:19-28.

18. Slough J, Cooney L, Brueckner M. Monocilia in the embryonic mouse heart suggest a direct role for cilia in cardiac morphogenesis. *Dev Dyn.* 2008;237:2304-2314.
19. Van der Heiden K, Hierck BP, Krams R, de Crom R, Cheng C, Baiker M, Pourquie MJBM, Alkemade FE, DeRuiter MC, Gittenberger-de Groot AC, Poelmann RE. Endothelial primary cilia in areas of disturbed flow are at the base of atherosclerosis. *Atherosclerosis.* 2008;196:542-550.
20. Groenendijk BCW, Hierck BP, Gittenberger-de Groot AC, Poelmann RE. Development-related changes in the expression of shear stress responsive genes KLF-2, ET-1, and NOS-3 in the developing cardiovascular system of chicken embryos. *Dev Dyn.* 2004;230:57-68.
21. Groenendijk BCW, Van der Heiden K, Hierck BP, Poelmann RE. The role of shear stress on ET-1, KLF2, and NOS-3 expression in the developing cardiovascular system of chicken embryos in a venous ligation model. *Physiology (Bethesda).* 2007;22:380-389.
22. Vennemann P, Kiger KT, Lindken R, Groenendijk BCW, Stekelenburg-de Vos S, ten Hagen TLM, Ursem NTC, Poelmann RE, Westerweel J, Hierck BP. *In vivo* micro particle image velocimetry measurements of blood-plasma in the embryonic avian heart. *J Biomech.* 2006;39:1191-1200.
23. Nakajima Y, Yamagishi T, Hokari S, Nakamura H. Mechanisms involved in valvuloseptal endocardial cushion formation in early cardiogenesis: roles of transforming growth factor (TGF)-β and bone morphogenetic protein (BMP). *Anat Rec.* 2000;258:119-127.
24. Goumans MJ, Lebrin F, Valdimarsdottir G. Controlling the angiogenic switch: a balance between two distinct TGFβ receptor signaling pathways. *Trends Cardiovasc Med.* 2003;13:301-307.
25. Goumans MJ, Valdimarsdottir G, Itoh S, Rosendahl A, Sideras P, ten Dijke P. Balancing the activation state of the endothelium via two distinct TGFβ type I receptors. *EMBO J.* 2002;21:1743-1753.
26. Goumans MJ, van Zonneveld AJ, ten Dijke P. Transforming growth factor-β-induced endothelial-to-mesenchymal transition: a switch to cardiac fibrosis? *Trends Cardiovasc Med.* 2008;18:293-298.
27. Zeisberg M, Neilson EG. Biomarkers for epithelial-mesenchymal transitions. *J Clin Invest.* 2009;119:1429-1437.
28. Arteaga CL, Hurd SD, Winnier AR, Johnson MD, Fendly BM, Forbes JT. Anti-transforming growth factor (TGF)β antibodies inhibit breast cancer cell tumorigenicity and increase mouse spleen natural killer cell activity. Implications for a possible role of tumor cell/host TGFβ interactions in human breast cancer progression. *J Clin Invest.* 1993;92:2569-2576.
29. Inman GJ, Nicolas FJ, Callahan JF, Harling JD, Gaster LM, Reith AD, Laping NJ, Hill CS. SB-431542 is a potent and specific inhibitor of transforming growth factor-b superfamily type I activin receptor-like kinase (ALK) receptors ALK4, ALK5, and ALK7. *Mol Pharmacol.* 2002;62:65-74.
30. Hierck BP, Molin DGM, Boot MJ, Poelmann RE, Gittenberger-de Groot AC. A chicken model for DGCR6 as a modifier gene in the DiGeorge critical region. *Pediatr Res.* 2004;56:440-448.
31. Haycraft CJ, Zhang Q, Song B, Jackson WS, Detloff PJ, Serra R, Yoder BK. Intraflagellar transport is essential for endochondral bone formation. *Development.* 2007;134:307-316.
32. Moyer JH, Lee-Tischler MJ, Kwon HY, Schrick JJ, Avner ED, Sweeney WE, Godfrey VL, Cacheiro NL, Wilkinson JE, Woychik RP. Candidate gene associated with a mutation causing recessive polycystic kidney disease in mice. *Science.* 1994;264:1329-1333.

33. Yoder BK, Richards WG, Sommardahl C, Sweeney WE, Michaud EJ, Wilkinson JE, Avner ED, Woychik RP. Differential rescue of the renal and hepatic disease in an autosomal recessive polycystic kidney disease mouse mutant. A new model to study the liver lesion. *Am J Pathol.* 1997;150:2231-2241.
34. Lehman JM, Michaud EJ, Schoeb TR, Ydin-Son Y, Miller M, Yoder BK. The Oak Ridge Polycystic Kidney mouse: modeling ciliopathies of mice and men. *Dev Dyn.* 2008;237:1960-1971.
35. Iomini C, Tejada K, Mo W, Vaananen H, Piperno G. Primary cilia of human endothelial cells disassemble under laminar shear stress. *J Cell Biol.* 2004;164:811-817.
36. Dekker RJ, van Thienen JV, Elderkamp YW, Seppen J, de Vries CJM, Biessen EAL, van Berkel TJ, Pannekoek H, Horrevoets AJG. Endothelial KLF2 links local arterial shear stress levels to the expression of vascular-tone regulating genes. *Am J Pathol.* 2005;167:609-618.
37. Dekker RJ, Van Soest S, Fontijn RD, Salamanca S, de Groot PG, VanBavel E, Pannekoek H, Horrevoets AJG. Prolonged fluid shear stress induces a distinct set of endothelial cell genes, most specifically lung Krüppel-like factor (KLF2). *Blood.* 2002;100:1689-1698.
38. McCormick SM, Eskin SG, McIntire LV, Teng CL, Lu CM, Russell CG, Chittur KK. DNA microarray reveals changes in gene expression of shear stressed human umbilical vein endothelial cells. *Proc Natl Acad Sci USA.* 2001;98:8955-8960.
39. Yan FF, Liu YF, Liu Y, Zhao YX. KLF4: a novel target for the treatment of atherosclerosis. *Med Hypotheses.* 2008;70:845-847.
40. Yoshida T, Kaestner KH, Owens GK. Conditional deletion of Krüppel-like factor 4 delays downregulation of smooth muscle cell differentiation markers but accelerates neointimal formation following vascular injury. *Circ Res.* 2008;102:1548-1557.
41. Mercado-Pimentel ME, Runyan RB. Multiple transforming growth factor-β isoforms and receptors function during epithelial-mesenchymal cell transformation in the embryonic heart. *Cells Tissues Organs.* 2007;185:146-156.
42. Combs MD, Yutzey KE. Heart valve development: regulatory networks in development and disease. *Circ Res.* 2009;105:408-421.
43. Yamagishi T, Ando K, Nakamura H. Roles of TGFβ and BMP during valvulo-septal endocardial cushion formation. *Anat Sci Int.* 2009;84:77-87.
44. Hierck BP, Van der Heiden K, Poelmann RE. Fluid shear stress and inner curve remodeling of the embryonic heart. Choosing the right lane! *ScientificWorldJournal.* 2008;8:212-222.
45. Zeisberg EM, Tarnavski O, Zeisberg M, Dorfman AL, McMullen JR, Gustafsson E, Chandraker A, Yuan X, Pu WT, Roberts AB, Neilson EG, Sayegh MH, Izumo S, Kalluri R. Endothelial-to-mesenchymal transition contributes to cardiac fibrosis. *Nat Med.* 2007;13:952-961.
46. Bisgrove BW, Yost HJ. The roles of cilia in developmental disorders and disease. *Development.* 2006;133:4131-4143.
47. McGrath J, Brueckner M. Cilia are at the heart of vertebrate left-right asymmetry. *Curr Opin Genet Dev.* 2003;13:385-392.
48. Marszalek JR, Ruiz-Lozano P, Roberts E, Chien KR, Goldstein LS. *Situs inversus* and embryonic ciliary morphogenesis defects in mouse mutants lacking the KIF3A subunit of kinesin-II. *Proc Natl Acad Sci USA.* 1999;96:5043-5048.
49. Icardo JM, Sanchez de Vega MJ. Spectrum of heart malformations in mice with *situs solitus, situs inversus*, and associated visceral heterotaxy. *Circulation.* 1991;84:2547-2558.
50. Kocaman O, Oflaz H, Yekeler E, Dursun M, Erdogan D, Demirel S, Alisir S, Turgut F, Mercanoglu F, Ecder T. Endothelial dysfunction and increased carotid intima-media thickness in patients with autosomal dominant polycystic kidney disease. *Am J Kidney Dis.* 2004;43:854-860.